Appl. Phys. B 59, 11–17 (1994)

Applied Physics B Lasers and Optics

Cooperative frequency locking and tristability in a class-B laser

G. Slekys*, K. Staliunas*, M.F.H. Tarroja, C.O. Weiss**

Physikalisch-Technische Bundesanstalt, Bundesallee 100, D-38116 Braunschweig, Germany
(Fax: +49-531/592-9292)

Received 11 February 1994/Accepted 10 March 1994

Abstract. The locking and unlocking phenomena of the modes of the transverse family $q=1$ in a CO_2 laser are investigated. The experimental results show three characteristic regions: a bistability between two helical waves of opposite handedness, a tristability among the two helicities of opposite handedness and an unlocked state, and the unlocked state. Near the locking threshold, oscillations which can be interpreted as due to the oscillations of the modal amplitudes and relative phase are also observed. These results are found to be consistent with solutions of the two-mode Maxwell-Bloch equations for class-B lasers.

PACS: 42.60.Jf, 42.65.−k, 61.70.Ga

When several transverse modes are excited in a laser, transverse dynamic phenomena can be observed. The occurrence of stationary patterns can be explained in terms of cooperative frequency locking within one or several transverse mode families. In such a case transverse modes of different optical frequencies lock to a common frequency producing a time independent pattern [1]. Stationary patterns for the transverse family $q=1$ to $q=3$ have been predicted and experimentally observed in class-A lasers [2]. For the $q=1$ family the stationary pattern can be a doughnut mode whose central dark region corresponds to a phase singularity (also referred to as an optical vortex) [2]. Other more complex stationary patterns of vortices have been observed such as an eight-vortex crystal-like structure in a sodium-dimer laser [3] and optical vortex lattices in a high fresnel number carbon-dioxide laser [4]. Multistability of stationary patterns has also been predicted [2]. This was demonstrated by the doughnut bistability in a HeNe laser [5] and multistability among $q=2$ patterns in a sodium laser [2].

Some transverse patterns exhibit temporal oscillations. Usually, these are attributed to the beating of modes. For example, the Gauss-Hermite modes, TEM_{01} and TEM_{10}, when not degenerate, result in an "unlocked doughnut" which shows regions in which the intensity pulses at the mode-beat frequency. In this case the non-degeneracy is primarily due to astigmatism, the reduction of which can lead to a locked state. The transition from the beating modes to the time-independent, locked state within the $q=1$ mode family was investigated in HeNe laser (class-A) [6].

Coexisting TEM_{00} and TEM^{*}_{01} modes results in a phase singularity revolving about the center of the laser beam. The "spinning vortex" spins at a frequency of the order of the difference of the mode-pulled frequencies of the two modes [7]. This dynamical pattern can serve as a good illustration of the hydrodynamic forces acting on optical vortices [8].

Contrary to class-A lasers, the inertia of population inversion plays a significant role in class-B lasers. Transverse pattern formation in this type of lasers (carbon-dioxide lasers, in particular) has been reported [9–12]. In [9–11] the spatiotemporal dynamics of the carbon-dioxide lasers was studied by changing the effective curvature of the resonator mirrors, and the pump, as the control parameters. The patterns observed are classified in symmetry groups and the changes in the patterns are interpreted by symmetry breaking. In [12], the emphasis is on the spatiotemporal behavior of slightly nondegenerate modes in the carbon-dioxide laser. In most cases, the temporal oscillations of the pattern are due to the beating of the excited modes but in some cases, these have been attributed to the modal amplitude oscillations [9].

In spite of extensive experiments a complete theoretical treatment of transverse dynamics in Class-B lasers is still missing. The theoretical analysis in [13, 14] also applies to class-A laser: the material variables (polarization and population inversion) have been adiabatically eliminated. Due to the adiabatic elimination the

* Permanent address: Dept. of Quantum Electronics, Vilnius University, Sauletekio av. 9, corp. 3, 2054 Vilnius, Lithuania
** Permanent address: National Institute of Physics, University of the Philippines, Quezon City, Philippines

phenomena characteristic for class-B lasers such as relaxation oscillations, antiphase mode beats [15], self-induced transverse dynamics [16] are excluded from the models in [13, 14].

In [17] the transverse mode dynamics has been investigated taking into account the inertia of population inversion, thus using the class-B laser model. The studies focused on transverse mode-locking unlocking phenomena. It was shown in particular, that the transverse mode locking, unlocking occurs as a subcritical bifurcation in contrary to the class-A laser, where locking is supercritical. As a consequence bistability between locked and unlocked states exists in class-B lasers.

This paper aims to confirm experimentally the predictions of [17]. In the following section the main results of the theory are summarized and applied to the family $q=1$. The experimental observations of the locking phenomena of the Hermite modes, TEM_{01} and TEM_{10}, in a carbon dioxide are presented.

1 Locking and unlocking of modes in class-B lasers

For class-A lasers, the polarization decay rate $\gamma_\perp$ and the population inversion decay rate $\gamma_\parallel$, are much larger than the field decay rate κ. Thus the polarization and population inversion can be adiabatically eliminated from the Maxwell-Bloch equations. In class-B lasers, $\gamma_\parallel \ll \kappa$ and the population inversion is not enslaved by the electric field. Its dynamics can, nevertheless, be incorporated using the modal approach [17] by expressing the population inversion $D(\mathbf{r}, t)$, in terms of the products of cavity modes $A_i(\mathbf{r}, t)$, with time dependent pump depletion amplitudes $d_{ij}(t)$. That is, $D(\mathbf{r}, t) = D_0(\mathbf{r})\left[1-\sum_{i,j} d_{ij}(t)\, A_i(\mathbf{r})\, A_j^*(\mathbf{r})\right]$, where $D_0(\mathbf{r})$ is the unsaturated population inversion. With the optical field amplitude expressed as $E(\mathbf{r}, t) = \sum_i f_i(t)\, A_i(\mathbf{r})$ (where $f_i(t)$ is the complex amplitude of the i-th cavity mode), the resulting equations for class-B lasers, considering only two modes, are [17]:

$$\frac{\partial f_1}{\partial t} = (D_1-\alpha_1)f_1 + \mathrm{i}\,\Delta\omega_1 f_1 - f_1(G_{11}d_{11}+G_{12}d_{22}) - f_2(G_{12}d_{12}+G'_{12}d_{21}), \tag{1a}$$

$$\frac{\partial f_2}{\partial t} = (D_2-\alpha_2)f_2 + \mathrm{i}\,\Delta\omega_2 f_2 - f_2(G_{22}d_{22}+G_{12}d_{11}) - f_1(G_{12}d_{21}+G'_{12}d_{12}), \tag{1b}$$

$$\frac{\partial d_{ij}}{\partial t} = -\gamma_\parallel(d_{ij}-f_i f_j^*), \tag{1c}$$

where α_i and $\Delta\omega_i$ are the linear loss and the frequency, respectively, of the i-th mode. $\gamma_\parallel$, α_i and $\Delta\omega_i$ are normalized here to κ. $D_i = \int\int D_0(\mathbf{r})\cdot|A_i(\mathbf{r})|^2\cdot d\mathbf{r}$ are the gain coefficients, and $G_{ij} = \int\int D_0(\mathbf{r})|A_i(\mathbf{r})|^2|A_j(\mathbf{r})|^2 d\mathbf{r}$ are the auto- and cross-saturation coefficients. $G'_{ij} = \int\int D_0(\mathbf{r}) A_i^2(\mathbf{r})A_j^2(\mathbf{r})d\mathbf{r}$ is the phase-sentive cross-saturation coefficient. A nonzero G'_{ij} results in a "nonlinear mode pulling" which causes the modes to lock for a range of values of their frequency difference. This "nonlinear mode pulling" is additional to the usual mode-pulling phenomenon (where the lasing frequency is a weighted average of the cavity frequency and gain line center frequency).

In the limit of $\gamma_\parallel \to \infty$, (1c) leads to $d_{ij} = f_i f_j^*$, and (1) transforms into the well-known mode-expansion equations for class-A lasers [2]:

$$\frac{\partial f_1}{\partial t} = (D_1-\alpha_1)f_1 + \mathrm{i}\,\Delta\omega_1 f_1 - f_1(G_{11}|f_1|^2 + 2G_{12}|f_2|^2 + G'_{12}f_1 f_2^*), \tag{2a}$$

$$\frac{\partial f_2}{\partial t} = (D_2-\alpha_2)f_2 + \mathrm{i}\,\Delta\omega_2 f_2 - f_2(G_{22}|f_2|^2 + 2G_{12}|f_1|^2 + G'_{12}f_2 f_1^*). \tag{2b}$$

Here coefficients G_{ij} are defined as in (1). In a more accurate analysis in [13, 14] the smallness of $\gamma_\parallel$ is taken into account by modifying the cross-saturation coefficients G_{ij}. We note, that such a way of taking the slowness of population inversion into account is correct in the limit $\varepsilon = \gamma_\parallel^{-1} \ll 1$ only, which is the limit of the class-A laser. For correct description of class-B lasers the inertia of population inversion must be taken into account by retaining (1c): only in this case the solutions of (1) describe properly the relaxation oscillations, which are characteristic for class-B lasers.

The presence of the additional (1c) changes the behavior of class-B lasers drastically from that of class-A lasers. Analysis of solutions of (1) for both types of lasers shows that the frequency of inter-mode beating in class-B lasers is always larger than that of the class-A laser. Furthermore, in the "mode non-pulling" case, $G'_{12}=0$ (for example, one which involves modes of different helicities), two transverse class-B laser modes always beat with nonzero frequency (i.e., the modes "anti-lock") [17]. This produces a nonstationary pattern even in the case where $\Delta\omega_1 = \Delta\omega_2$, in which case class-A lasers emit a stationary pattern. The frequency of these self-induced oscillations is of the order of magnitude of the relaxation oscillation frequency. Bistability between different regimes – different solutions of (1) – also appear for $|\Delta\omega_1 - \Delta\omega_2| \leq \omega_{\mathrm{rel}}$.

Bistability occurs also when locking modes are frequency-pulled. This is shown in the frequency locking, unlocking behavior of the two Gauss-Hermite modes TEM_{10} and TEM_{01} in Fig. 1. For these particular modes and in the case of spatially uniform pump $D_1 = D_2 = D_0$, $G_{11} = G_{22} = 3/(4\pi)$ and $G_{12} = G'_{12} = 1/(4\pi)$. The figure shows the dependence of the beat frequency on the difference between the single-mode frequencies of class-A and class-B lasers. Although these modes belong to the same family and in the ideal case are frequency-degenerate, imperfect rotational symmetry in the cavity

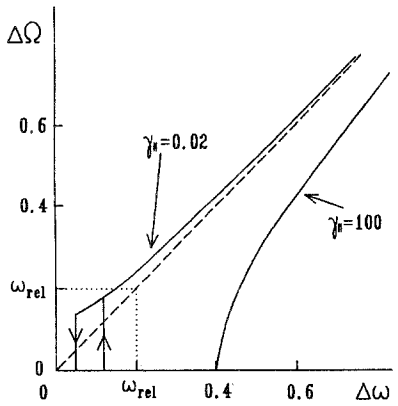

Fig. 1. The beat frequency $\Delta\Omega$ vs mode frequency separation $\Delta\omega$ for class-A ($\gamma_\parallel = 100$), and class-B ($\gamma_\parallel = 0.02$) lasers obtained from the numerical solution of (1) for $D_0 = 2$

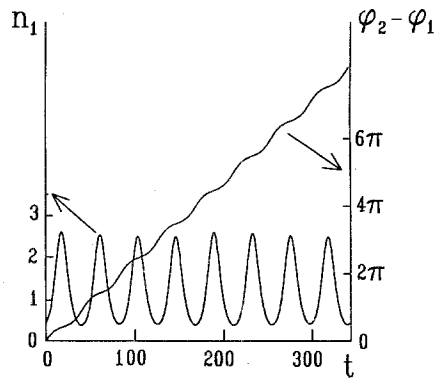

Fig. 2. The temporal dynamics of the phase difference of the modes $\Delta\varphi = \varphi_1 - \varphi_2$, and of the mode intensity $n_1 = n_2 = |f_1|^2$ obtained from the numerical solution of (1) for $\gamma_\parallel = 0.02$ and $D_0 = 2$

can lift this degeneracy, justifying the separate frequency assignments, $\Delta\omega_1$ and $\Delta\omega_2$, to the two modes. As Fig. 1 suggests, in class-A lasers, the modes can lock even in the presence of a certain degree of rotational asymmetry. From (1) this locking frequency is found to be $\Delta\omega_{\text{lock}} = 0.4(D_0 - 1)$ [17]. The locking occurs as a supercritical bifurcation when parameter $\Delta\omega$ is changed in class-A lasers.

In class-B lasers the locking occurs as a subcritical bifurcation, differently from class-A laser. Thus a region of coexistence between locked and unlocked modes exists. Compared with class-A lasers, locking occurs at a significantly smaller mode frequency difference, $\Delta\omega$, which is of the order of magnitude of the relaxation oscillation frequency: $\omega_{\text{rel}} = [2\gamma_\parallel(D_0 - 1)]^{1/2}$. Thus it is more difficult to obtain frequency locking in class-B than in class-A lasers. In the coexistence region of locked and unlocked states, the locked state can have either right-hand or left-hand helicity. Hence this bistable region is actually tristable.

Relaxation oscillations plays an important role in the locking of class-B lasers. Specifically, the numerical calculations suggest that the mode locking in the bistable regime (i.e., the jump from the upper to the lower branch of Fig. 1) is the result of the synchronization between the mode-beat frequency, and the first subharmonic of the relaxation oscillation frequency. Near the locking threshold the modal amplitudes are themselves oscillating at a frequency equal to the relaxation oscillation, as shown in Fig. 2. The relative phase between the modes (also shown in Fig. 2) shows oscillatory time dependence with values of odd multiples of $\pi/2$ at the modal amplitude maxima. Increasing $\Delta\omega$, from the locked branch, unlocking occurs when the mode-locked solution of (1) becomes unstable. The linear stability analysis [17] shows that the mode unlocking occurs for $\Delta\omega > [\gamma_\parallel(D_0 - 1)]^{1/2}$.

Experimentally the locking mechanism can be explored by perturbing the cavity (for example by introducing loss in a form of a spot or a pin). Losses have two possible effects. One is spatial distortion (or equivalently, nonuniform phase changes) of the beam. This results in changes in the frequencies of the active modes. For illustration the frequency shift due to the introduction of an aperture arranged rotationally symmetrically around the TEM^*_{01} Gauss-Laguerre mode (doughnut) is calculated (see Appendix). The result is $\Delta\omega_{\text{dif}} = \lambda^2/(4\,\Delta\omega_\perp)$, where λ is the parameter of additional loss due to the aperture, and $\Delta\omega_\perp$ is the frequency separation of the transverse modes.

The second effect of the introduction of losses, is related to the usual frequency-pulling. The greater the loss, the more pulled is the actual lasing frequency towards the gain line center. An additional loss introduces a frequency shift, $\Delta\omega_{\text{pul}}$, given by: $\Delta\omega_{\text{pul}} = \lambda\,(\omega_A - \omega_C)\,\gamma_\perp/(1+\gamma_\perp)^2$, where ω_A is the gain line center frequency, and ω_C is the frequency of the mode (see Appendix).

The first mechanism always increases the excited-mode frequency. The second mechanism, on the other hand, always pulls the frequency of the mode towards the center of the line. For CO_2 lasers both effects are of the same order of magnitude. When the mode frequency ω_C is less than the gain line center frequency ω_A, ($\omega_C < \omega_A$), the effects of the two mechanisms add. Thus the mode is more tunable in this case than when its frequency is larger than ω_A, where the effects subtract.

The loss can be restricted to affect only one of the modes. It can be changed to allow a continuous variation of $\Delta\omega$ (which include the two loss-induced frequency shifts discussed above as well as that induced by the astigmatism of the cavity).

2 Experiment

Experimentally locking and unlocking of the Hermite modes TEM_{01} and TEM_{10} is observed in a carbon-dioxide laser, schematically shown in Fig. 3.

The CO_2 laser consists of tube which is 55 cm long and has an 8 mm inner diameter, a curved mirror with a radius of curvature of 2 m and a 150 lines/mm plane (outcoupling) grating with a 95% diffraction efficiency. With the gain bandwidth of approximately 100 MHz, and with a cavity length of 0.8 m, the laser oscillates in a single longitudinal mode. The transverse mode separation and the cavity linewidth are 41 MHz and 15 MHz,

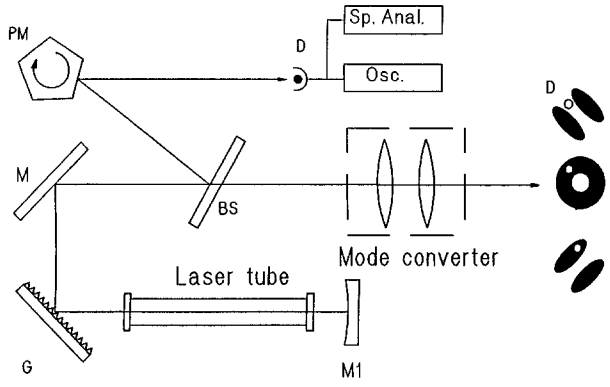

Fig. 3. Experimental setup. M1: concave Mirror; M: plane Mirror, BS: BeamSplitter; G: Grating, PM: rotating Polygon Mirror; D: Detector. The 3 possible patterns after the mode converter are shown. ○ indicates the position of the detector in the pattern

respectively. It was possible to restrict the laser to selective oscillation in the $q=1$ family to be comparable with the theoretical two-mode model. The tuning is achieved by the fine adjustment of the cavity length using a piezoelectric transducer to which the mirror is attached.

For measurements, the laser radiation is detected by a fast HgCdTe detector and the resulting signal is displayed simultaneously on an osciloscope and a spectrum analyzer. The spatial-temporal dependence of the intensity along a cut in the pattern is monitored using a rotating mirror.

For sufficiently large frequency difference, $\Delta\omega$, between the modes TEM_{01} and TEM_{10} (for example in the presence of Brewster windows), the "nonlinear mode pulling" discussed above plays a very insignificant role. In this case, the total optical field in the overlapping regions of two Hermite modes is just the sum of the electric fields of the modes. When modes are of different frequencies, the intensity in the overlap regions is modulated at the beat frequency [9, 10, 12]. This is shown schematically in Fig. 4a. The unlocked state consists of superimposed TEM_{10} and TEM_{01} modes whose electric field directions are indicated by the arrows. The overlapping regions are indicated by A, B, C, and D. It is straightforward to calculate the intensity in the overlapping regions and to show that the intensity in region A oscillates in phase with D and anti-phase with region C. Intensity pulsations in the overlap regions are shown in Figs. 4b, c, which are the beam scans of intensity across the lines passing through A and B and through A and D, respectively. In the nodal lines of the Hermite modes (1 and 2 cuts in Fig. 4a) there are no significant temporal variations of intensity as would be expected because these are regions where the modes do not overlap.

To explore the locking and unlocking bistability, Brewster windows were replaced by plane ZnSe windows. To allow continuous change of the mode frequency difference, losses for one of the Hermite modes are introduced by translating a pin in either of the two directions (indicated as 1 or 2 in Fig. 4a). As discussed in Sect. 1, the losses can cause pulling of modes and distortion of the beam with the effect of compensating for

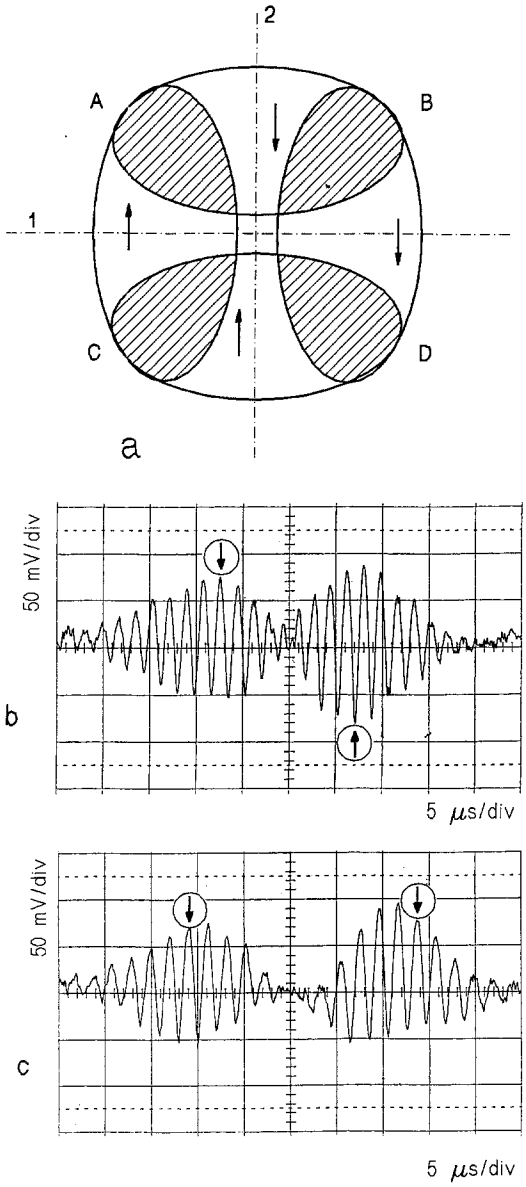

Fig. 4. a Superposition of TEM_{01} and TEM_{10} modes indicating the directions of the electric field of modes. A, B, C, D are the regions where the modes overlap. 1- and 2-axes correspond to the nodal lines of Hermite TEM_{01} modes. The cross sections of the unlocked doughnut pattern show the temporal intensity modulation for (**b**) A–B cut (antiphase oscillation) and (**c**) A–D cut (in-phase modulation). The time interval between the arrows in (**b**) and (**c**) represents an integral multiple of the beating period

residual astigmatism [6]. Both effects are achieved by a pin whose position can be used as a control parameter. The effect of changing of the pin position (along direction 1 of Fig. 3) on the beat frequency of the lasing modes is shown in Fig. 5. By translating the pin along either 1 or 2 the loss in one of the two Hermite modes can be changed. The frequency tuning is achieved and consequently, the modes can be locked or unlocked. The zero position of the pin is a point sufficiently far from the beam and corresponds to a locked "doughnut" state.

From the locked state ($r=0$), the pin is translated towards the beam. At a pin position $r=6.5$ mm, the

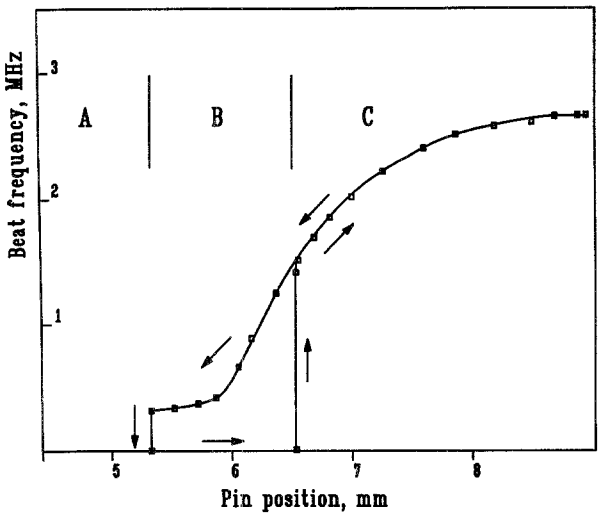

Fig. 5. Beat frequency vs pin position

pattern unlocks. Similarly, from the unlocked state the pin translation is reversed (i.e., the pin is moved away from the pattern). As r decreases, the doughnut remains unlocked until a critical value of the beat frequency (approximately equal to 300 kHz), beyond which the doughnut locks (at $r = 5.3$ mm). This beat frequency is of the order of the relaxation oscillation frequency. The different thresholds for locking and unlocking represent a bistability which is evident in Fig. 5. The tunability of the mode frequency due to the losses (and consequently the range B of Fig. 5) depends on which side of the gain profile the mode frequency is located. This is consistent with the theoretical prediction discussed in the previous section.

The previous theoretical discussion has also pointed out that modal amplitudes and the relative phase of the modes are oscillating near the locking threshold. This is confirmed experimentally as shown in Fig. 6 where the power spectra at two points in the pattern are shown. Fig. 6a is a typical power spectrum in regions A, B, C, and D (of Fig. 4a) where the two Hermite modes overlap. In the regions where only one of the modes is present, the power spectrum (Fig. 6b) shows strong oscillation at a frequency equal to the second harmonic of the beat frequency. These second-harmonic oscillations are indicative of the modal oscillations as predicted for the region near the locking threshold. This can be seen in Fig. 6c, d which show the intensity peaks associated with the ordinary beating of the modes (Fig. 6c) and the modal oscillations (Fig. 6d) in the pattern. The intensity oscillation at the second harmonic of the beat frequency is independent on the angular location.

In the vicinity of the locking point the second harmonic of the beat, related also to the modal oscillation, increases and through resonance with the relaxation oscillation leads to the locking of the modes.

As pointed out in the previous section the bistable region of locking and unlocking (region B in Fig. 5) is actually tristable corresponding to unlocked doughnut and two locked doughnuts of opposite helicities. To

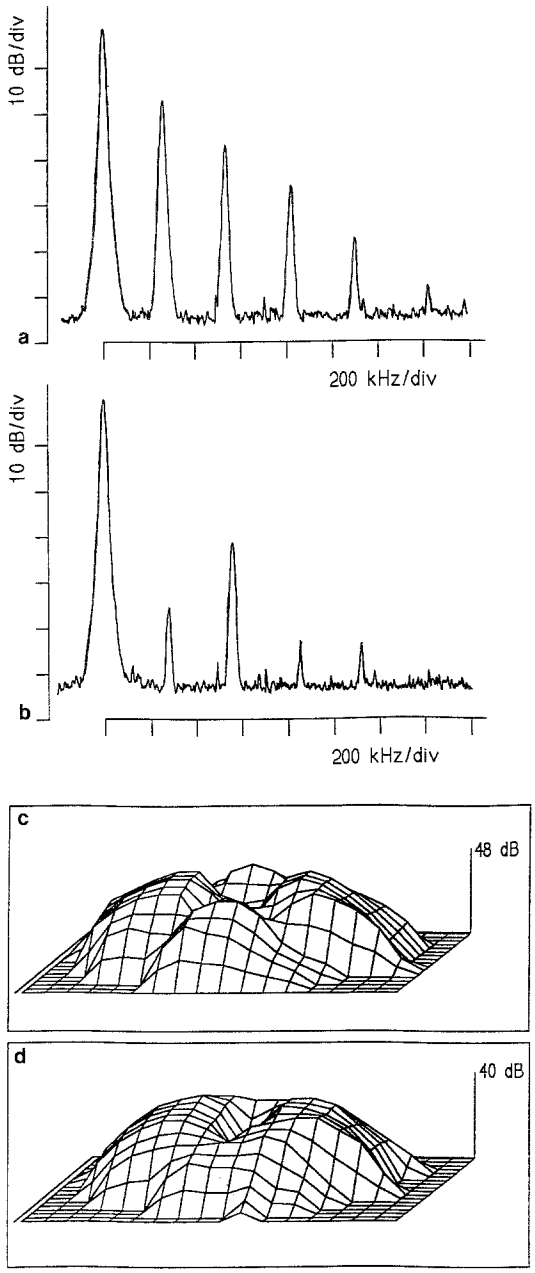

Fig. 6a–d. Power spectra in the pre-locking state when the detector is in (**a**) the overlap region A, and (**b**) the nodal line 1 (in Fig. 4a). The distribution of the beat amplitude (**c**) and the amplitude of the second harmonic of the beat (**d**)

show this, a part of the beam is passed through a mode converter consisting of two cylindrical lenses. This mode converter changes a left- (right-) handed locked doughnut into a Hermite TEM_{01} (TEM_{10}) modes tilted by 45° [5]. Thus by placing the detector behind the converter in the nodal line of the Hermite mode TEM_{01} as shown in Fig. 3, we can relate the high-level signal to the right-handed helical emission, the low-level signal to the left-handed helicity, and the intermediate level to the unlocked state. Following the technique used in showing bistability in the HeNe laser [5], the laser was turned on and off periodically and the result of such switch-on statistics is shown in Fig. 7. In region A (of Fig. 5), the

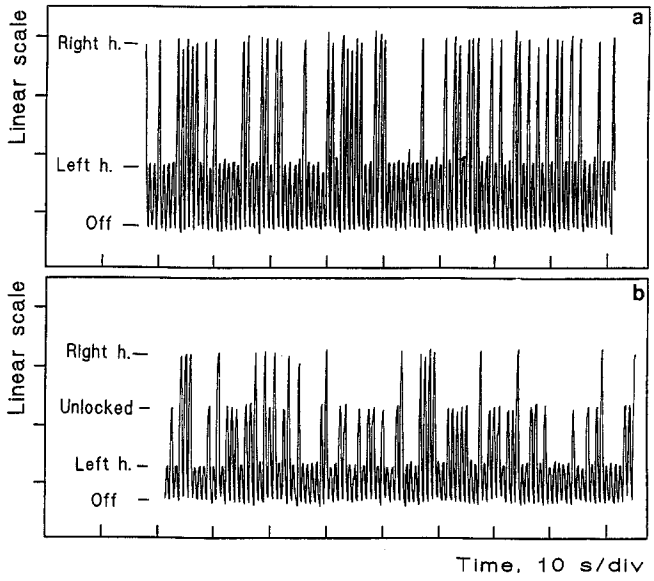

Fig. 7a, b. Statistical realizations of the laser states depending on the loss parameter in (**a**) bistable region A and (**b**) tristable region B of Fig. 5

laser switches randomly between the right-hand and left-hand helicity as shown in Fig. 7a. Fig. 7b which corresponds to region B shows tristability. In region C the trivial case of an unlocked doughnut is observed (called in [11] a modulated wave).

Depending on the angular position of the losses introduced, it is also possible to make the laser operate in a prefered helicity. In this case one of the helical states is suppressed and in region B the laser shows bistability between the prefered helicity doughnut and the unlocked state.

3 Conclusions

We have experimentally conformed the theoretical prediction [17] that the locking and unlocking phenomena of the Gauss-Hermite modes, TEM_{01} and TEM_{10}, in CO_2 lasers are characterized by the coexistence of locked and unlocked states. It was also proved that this region corresponds to tristability of an unlocked doughnut, a doughnut with right-handedness and a doughnut with a left-handedness. In the locking region, the bistable doughnut state was observed. The locking behavior was shown to be influenced by the population inversion dynamics which is important in class-B lasers.

Acknowledgements. This work was supported by Deutsche Forshungsgemeinschaft and ESPRIT project 7118 (TONICS). M.F.H. Tarroja is a recipient of the Alexander von Humboldt fellowship. The authors thank Chr. Tamm for meaningful discussions.

Appendix

Mode-Frequency Shifts due to Spatially Inhomogeneous Loss

The equation for transverse modes of the cavity with spherical mirrors is:

$$\frac{\partial A}{\partial t} = -\mathrm{i}\,\Delta\omega_\perp\, r^2 A + (\mathrm{i}\,\Delta\omega_\perp/4)\nabla^2 A, \tag{A1}$$

where $\Delta\omega_\perp$ is the transverse mode frequency separation and $\nabla^2 = \partial_x^2 + \partial_y^2$ is the Laplacian operator in a two dimensional space (x, y) or (r, φ). The solutions of (1a) are the Gauss-Laguerre functions, and the first two are:

$$A_0(\mathbf{r}, t) = (2/\pi)^{1/2} \exp(-r^2) \exp(-\mathrm{i}\,\Delta\omega_\perp t), \tag{A2a}$$

$$A_1(\mathbf{r}, t) = 2\,\pi^{-1/2} r \exp(-r^2 \pm \mathrm{i}\,\varphi) \exp(-2\mathrm{i}\,\Delta\omega_\perp t). \tag{A2b}$$

To evaluate the effect of an aperture on the solution (A2b) a term describing the presence of a spatially inhomogeneous loss is introduced in (1a) as follows:

$$\frac{\partial A}{\partial t} = (-r^2/r_\mathrm{p}^2)\, A - \mathrm{i}\,\Delta\omega_\perp\, r^2 A + (\mathrm{i}\,\Delta\omega_\perp/4)\,\nabla^2 A. \tag{A3}$$

For convenience the loss function is of parabolic form, where r_p corresponds to the radius of the aperture.

A solution of (A3) of the following form is assumed:

$$A_1(\mathbf{r}, t) = r \exp(-r^2/r_0^2 + i\,r^2/R_0^2 \pm \mathrm{i}\,\varphi) \times \exp(-\mathrm{i}\,\omega t - \lambda t), \tag{A4}$$

where r_0 is the radius of the beam, which is not equal to 1 as in (A2), R_0 is the parameter of the laser beam curvature, and λ is the loss parameter. After (A4) is inserted into (A3), and the terms with the equal powers of r are collected, the following relations are obtained:

$$\begin{aligned} &\lambda = 2\,\Delta\omega_\perp/R_0^2, \qquad \omega = -2\,\Delta\omega_\perp/r_0^2, \\ &R_0^2/r_\mathrm{p}^2 = 2\,\Delta\omega_\perp/r_0^2, \qquad r_0^{-4} - R_0^{-4} = 1. \end{aligned} \tag{A5}$$

From relations (A5) the unknown parameters r_0, R_0, ω and λ are determined. The mode frequency ω is no longer equal to $-2\,\Delta\omega$ as in (A2b), and in the limit of $2\,\Delta\omega\, r_\mathrm{p}^2 \gg 1$ (i.e., with small influence of aperture), the frequency and the decay rate of the mode are connected by a simple relation. Thus, the frequency shift due to the aperture $\Delta\omega_\mathrm{dif}$ is

$$\Delta\omega_\mathrm{dif} = \omega - 2\,\Delta\omega_\perp = \lambda^2/(4\,\Delta\omega_\perp), \tag{A6}$$

which is the analogue of the Kramers-Kronig relation for the spatial spectrum.

According to (A6) the mode frequency increases with increasing losses due to the aperture, λ. Another effect of the presence of the aperture is related to frequency pulling. The spatially distributed losses decrease the quality of the resonator for the particular mode, and the frequency pulling changes. The frequency of the laser radiation, ω, is the weighted average of the central frequency of the amplification line, ω_A, and the mode frequency, ω_C. That is, $\omega = (\omega_\mathrm{C}\kappa + \omega_\mathrm{A}\gamma_\perp)/(\kappa + \gamma_\perp)$, where the re-

laxation rate of the optical field is $\kappa = 1+\lambda$ [λ is the additional loss due to the aperture as in (A4–6]. For $\lambda \ll 1$, the frequency shift is:

$$\Delta\omega_{\text{pul}} = \lambda \frac{\gamma_\perp}{(1+\gamma_\perp)^2}(\omega_A - \omega_C). \tag{A7}$$

The frequency change due to this phenomenon is directed towards the amplification line center when the losses increase.

References

1. L.A. Lugiato, C. Oldano, L.M. Narducci: J. Opt. Soc. Am. B **5**, 879 (1989)
2. M. Brambilla, L.A. Lugiato, V. Penna, F. Prati, C. Tamm, C.O. Weiss: Phys. Rev. A. **43**, 5090 (1991)
3. W. Klische, C.O. Weiss, B. Wellegehausen: Phys. Rev. A **39**, S19 (1989)
4. D. Dangoisse, D. Hennequin, C. Lepers, E. Louvergneaux, P. Glorieux: Phys. Rev. A **46**, 5955 (1992)
5. C. Tamm, C.O. Weiss: J. Opt. Soc. Am. B **7**, 1034 (1990)
6. C. Tamm: Phys. Rev. A **38**, 5960 (1988)
7. M. Brambilla, M. Cattaneo, L.A. Lugiato, R. Pirovano, F. Prati, A.J. Kent, G.-L. Oppo, A.B. Coates, C.O. Weiss, C. Green, E.J. D'Angelo, J.R. Tredicce: Phys. Rev. A **49**, 1452 (1994)
8. C.O. Weiss: Phys. Rep. **216**, 311 (1992)
9. J.R. Tredicce, E.J. Quel, A.M. Ghezzawi, C. Green, M.A. Pernigo, L.M. Narducci, L.A. Lugiato: Phys. Rev. Lett. **62**, 1274 (1989)
10. C. Green, G.B. Mindlin, E.J. D'Angelo, H.G. Solari, J.R. tredicce: Phys. Rev. Lett. **65**, 3124 (1990)
11. E.J. D'Angelo, E. Izaguirre, G.B. Mindlin, G. Huyet, L. Gil, J.R. Tredicce: Phys. Rev. Lett. **68**, 3702 (1992)
12. D. Hennequin, C. Lepers, E. Louvergneux, D. Dangoisse, P. Glorieux: Opt. Commun. **93**, 318 (1992)
13. H.G. Solari, R. Gilmore: J. Opt. Soc. Am. B **7**, 828 (1990)
14. R. Lopez-Ruiz, G.B. Mindlin, C. Perez-Garcia: Phys. Rev. A. **47**, 500 (1993)
15. K. Otsuka: Phys. Rev. Lett. **67**, 1090 (1991)
16. C.O. Weiss, H.R. Telle, K. Staliunas, M. Brambilla: Phys. Rev. A **47**, 1616 (1993)
17. K. Staliunas, M.F.H. Tarroja, C.O. Weiss: Opt. Commun. **102**, 69 (1993)